Applied Mathematical Modelling 35 (2011) 1581–1590

Contents lists available at ScienceDirect

Applied Mathematical Modelling

journal homepage: www.elsevier.com/locate/apm

Short-wave instabilities on a vortex pair of unequal strength circulation ratio

Joine So, Kris Ryan *, Gregory J. Sheard

Fluids Laboratory for Aeronautical and Industrial Research (FLAIR), Department of Mechanical and Aerospace Engineering, Monash University, VIC 3800, Australia

ARTICLE INFO

Article history:
Received 1 September 2010
Accepted 20 September 2010
Available online 8 October 2010

Keywords:
Vortex interaction
Vortex adaptation
Perturbation analysis
Kelvin modes
Crow instability

ABSTRACT

The creation of vortex pairs occurs in a range of industries, including mixing, transport, and plastic moulding. In particular, vortex pairs are observed in the wake of aircraft, and are the cause of a significant hazard in the aviation industry. Instabilities, which grow on vortex pairs, have the potential to lead to enhanced dissipation, thus limiting this safety concern, in addition to enhancing mixing in chemical engineering industries. To date research has mostly considered instabilities growing on a vortex pair where each vortex has the same magnitude of circulation. However, in practice it is unusual to have an equal-strength vortex pair. This investigation is the first to consider the instability modes that may develop on a Lamb–Oseen vortex pair of arbitrary circulation ratio. We find a significant change in the growth rates of all instability modes reported previously for an equal-strength vortex pair. All simulations employ an accurate spectral-element method to discretise the domain coupled with a three-step time splitting scheme. A wide range of instability wavelengths is considered to ensure that all instability modes are captured. By identifying and enhancing the leading instability modes, we are able to enhance the dissipation of the vortex pair.

1. Introduction

The stability of vortex pairs to linear perturbations have been the subject of intense study for several decades, due largely to the application of these findings in the enhanced dissipation of aircraft wakes, and an improvement in our understanding of the interaction of individual vortex filaments within turbulent flows [1].

Much of this work has concentrated on perturbations growing on vortex pairs where the circulation of each vortex is equal in magnitude. Leweke and Williamson [2] experimentally considered an equal strength magnitude, counter-rotating vortex pair, finding both a long-wave (Crow) mode [3] and a short-wave (Kelvin) mode [4], growing on the vortex pair. Laporte and Corjon [5] revisited the investigation with direct numerical simulations to investigate the interactions between the Crow and the short-wave instabilities. Both [2,5] found that the interaction of the two instability modes substantially decreased the time for the vortex pair to dissipate. In particular, the short-wave instability developed cooperatively on both vortices [2,5]. This "cooperative" mechanism significantly enhanced the mixing between the vortices, when compared to the situation with only the Crow instability developing.

The short-wave Kelvin mode is also commonly described as an elliptic instability. The term "elliptic" describes the vortex profile when deformed under the strain induced by the other vortex. The elliptic profile is crucial for the vortex to be susceptible to the growth of three-dimensional, Kelvin type perturbations. Pierrehumbert [6] identified this instability as a three-dimensional short-wave instability for a simple two-dimensional elliptic inviscid flow, while Bayly [7] provided a

* Corresponding author.
E-mail addresses: Joine.So@monash.edu (J. So), Kris.Ryan@monash.edu.au, kris.ryan@eng.monash.edu.au (K. Ryan), Greg.Sheard@monash.edu (G.J. Sheard).

0307-904X/$ - see front matter © 2010 Elsevier Inc. All rights reserved.
doi:10.1016/j.apm.2010.09.034

supporting theoretical framework. This type of short-wave instability was independently observed for a vortex ring by Widnall and Sullivan [8], and the mechanisms controlling the instability were explained in detail through an analytical model [9]. The analytical model required knowledge of the internal profile of the vortex to be known. Widnall et al. [9] also claimed that the same kind of instability could occur in other flow structures (for example a vortex pair). This claim was supported by Tsai and Widnall [4]. A comprehensive review of elliptic instability theory may be found in [10].

By comparison with equal-strength vortex pairs, relatively little work has considered vortex pairs of unequal circulation strength. Ortega et al. [11] experimentally considered unequal-strength counter-rotating vortex pairs formed in the wake of a specific wing planform. The use of their specific wing planform restricted the range of circulation strength ratios they could consider. They observed several three-dimensional instability modes growing on the vortex cores, however little description of the modes was provided. [12], following the work of [3,13], developed an analytical model to consider instabilities which may grow on a vortex pair of unequal strength circulation. However, the model was restricted to consider only large wavelength, sinuous instabilities, and did not consider the effect that the vortex profile will have on the instability modes that could form. Comparing their results with [11], several discrepancies were noted, especially where instability modes were of short wavelength.

Many investigations (for example, [4,14]) have considered the instabilities that may grow on a vortex pair by considering an isolated vortex immersed within a linear strain field, the strain field being carefully chosen such that it is equivalent to the presence of a nearby vortex. These investigations have identified a range of Kelvin modes that can alter the profile of the vortex core. The analytical investigation of [14], who considered an isolated vortex immersed within a strain field, has shown that the magnitude of strain at the center of a vortex is directly proportional to the instability growth rate. However, findings using this technique are limited, as the technique assumes that the strain field is vanishingly small and the vortex core remains axi-symmetric and retains a perfectly elliptic profile.

Sipp and Jacquin [15] conducted a linear stability investigation for a counter-rotating vortex pair, of equal-strength vortices. They defined the most unstable mode predicted as the principal mode $(-1,1)$, which was observed in [2,5]. Lacaze et al. [16] found other Kelvin instability modes, besides the principal mode $(-1,1)$, to be more unstable when an axial component is added to the baseflow vortex (not considered here). The other dominant Kelvin modes feature a temporally rotating perturbation field, and the vortex core is twisted axially into a helical structure. This is in contrast to the sinusoidal stationary core of a vortex perturbed with the mode $(-1,1)$. The mode shape notation in brackets follows the classic work of [17], who first described the vibrations of a columnar Rankine vortex and provided the solution for an inviscid flow.

Ref. [18] have shown that counter-rotating unequal-strength vortex pairs typically lead to higher strain rates measured at the core of the weaker vortex than its counterpart. When the strength difference of the two vortices is extreme, the weaker vortex undergoes significant deformation and its overall topology becomes a crescent shape. The analytical model of [14] may not be well applicable to predict the instability in this situation for the weak vortex cannot be well described by an elliptical profile.

In this study, we will consider several pairs of unequal-strength counter-rotating vortices. Key to our investigation is to identify if the Kelvin modes identified in prior studies grow in our highly deformed vortex cores, or if new instability modes dominate the flow. These results will have direct application to the aviation field as unequal strength vortex clusters feature prominently in the wake of an aircraft.

Comparisons between previous analytical solutions and the present work's numerical findings will be provided to validate the numerical findings. A-priori we may expect that for small Λ (a ratio of the weak vortex circulation to the strong vortex circulation), instabilities will grow preferentially on the weaker vortex (due to the increased strain on the vortex).

1.1. Flow field description

In this study two counter-rotating Lamb–Oseen vortices, each of characteristic radius a, are placed a distance b apart as shown in Fig. 1. Initially, each vortex is defined in isolation with a Lamb–Oseen profile, which has a vorticity field defined as

$$\omega_{axial} = \frac{\Gamma}{\pi a_0^2} e^{-\left(\frac{r}{a_0}\right)^2}, \tag{1}$$

where Γ is the circulation of the vortex, a_0 is the initial vortex radius, and r is the radial dimension. For all simulations discussed here the length-scale ratio is initially set to $a_0/b = 0.25$. The circulation strength ratio may be defined as

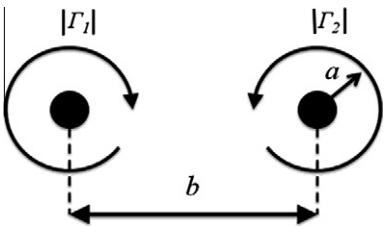

Fig. 1. Schematic diagram of the vortex pair.

$$\Lambda = \frac{\Gamma_1}{\Gamma_2}, \tag{2}$$

where Γ_1 is the circulation of the weaker vortex and Γ_2 is the circulation of the stronger vortex. In this study we have restricted our attention to $-0.1 \geqslant \Lambda \geqslant -1.0$. The effect of viscosity may be quantified through the Reynolds number $Re = \Gamma_2/\nu$ based on the circulation of the strongest vortex, where ν is kinematic viscosity. Viscous effects act to increase the radius of each vortex core (see, [14] for details); this effect may be approximated to first order through the equation

$$a(t) = \sqrt{a_0^2 + 4\nu t}, \tag{3}$$

where t is time.

For all simulations, the Reynolds number was set to 20,000, to agree with the previous studies of [14], and to minimize the impact of viscous radial growth. In addition, the initial core radii are equal for both vortices at the commencement of all simulations considered in this study. It should be noted that viscous forces will be more dominant in the vicinity of the weaker vortex, leading the core radius of the weak vortex to grow substantially more than the radius of the strong vortex at low $|\Lambda|$. The discrepancy in core radii is important as work by Le Dizès and Laporate [14] and Lacaze [16], considering a single vortex immersed in a strain field, have shown that the instability wavenumber, k should be normalized by core radius. Under the assumption that instabilities will grow preferentially in the weak vortex, it is this core radius that is most important. In this investigation we normalize k with the initial vortex core size a_0.

1.2. Numerical technique

There are two stages comprising the overall technique. The first stage involves evolving the two-dimensional base flow field from the initial condition of two superimposed isolated Lamb–Oseen vortices (not a solution of the Navier–Stokes equations) to a mutually deformed quasi-steady state by solving the incompressible Navier–Stokes equations

$$\begin{aligned} &\tfrac{\partial \mathbf{u}}{\partial t} + (\mathbf{u}\cdot\nabla)\mathbf{u} = -\nabla p + \nu\nabla^2\mathbf{u}, \\ &\nabla\cdot\mathbf{u} = 0, \end{aligned} \tag{4}$$

where $\mathbf{u}(x,y,t)$ is the two-dimensional velocity vector, and p is the kinematic static pressure. This relaxation process, leading towards the quasi-steady state, has been described in detail for equal strength vortex pairs by Le Dizès and Verga [19] for co-rotating vortices, and [15] for counter-rotating vortices. More recently, [18,20] have considered the case of $|\Lambda| \neq 1$. Following the standard approach for stability analysis of vortex pairs [16], a frozen snapshot of the flow when the vortices have adapted to each other, serves as a basis for the second stage of the technique (linear stability analysis). This effectively eliminates the growth of the vortex core through viscous diffusion during the stability analysis.

The growth-rate and mode-shape of linear perturbations acting on the adapted vortex pair are then calculated through the solution of the linearized Navier–Stokes equations. By freezing the two-dimensional flow field, the perturbation field is effectively rotating at the same rate as the vortex pair. The rotation rate and center of rotation of the vortex pair may be calculated analytically (see for example [14]), or through direct measurement, as was the case here. This rotation is accounted for by solving the linearized Navier–Stokes questions in a non-inertial reference frame, fixed to the frozen two-dimensional field, these equations are defined as:

$$\begin{aligned} &\tfrac{\partial \mathbf{u}'}{\partial t} + (\mathbf{U}_{\mathrm{rel}}\cdot\nabla)\mathbf{u}' + (\mathbf{u}'\cdot\nabla)\mathbf{U}_{\mathrm{rel}} = -\nabla p' + \nu\nabla^2\mathbf{u}' - 2\Omega\times\mathbf{u}', \\ &\nabla\cdot\mathbf{u}' = 0 \end{aligned} \tag{5}$$

where $\mathbf{u}'(x,y,z,t)$ and $p'(x,y,z,t)$ are the three-dimensional perturbation velocity and pressure components, and $\mathbf{U}_{\mathrm{rel}} = (\mathbf{U} - \Omega\times R)$ is the relative velocity of the frozen base flow on the non-inertial frame, where Ω is the self-rotation rate (which may be approximated as $(\Gamma_1 + \Gamma_2)/2\pi b^2$) and R is the radial distance measured from the instantaneous center of self-rotation for the two vortices in the base flow. The last term in the first equation of Eq. (5) is the correction for the Coriolis effect in the non-inertial reference frame. This process assumes the perturbation velocity and pressure terms may be written in the general form

$$P' = \widehat{P}(x,y)e^{ikz + i\sigma t}, \tag{6}$$

where P' represents any of the perturbation components (u',v',w') and p'; $\widehat{P}$ is the mode shape, k is the wavenumber of the instability along the axis of the unperturbed vortex pair, and σ is the perturbation growth rate. In practice, a normalized growth rate, $\sigma^* = \sigma\cdot t_c$, is considered where

$$t_c = \frac{2\pi b^2}{|\Lambda|\Gamma_2}, \tag{7}$$

is the time taken for the strong vortex to travel a distance b along its path. The general perturbation form of Eq. (6) is substituted into the linearized Navier–Stokes Eq. (5), leading to a sparse-matrix eigenvalue problem. The leading instability mode

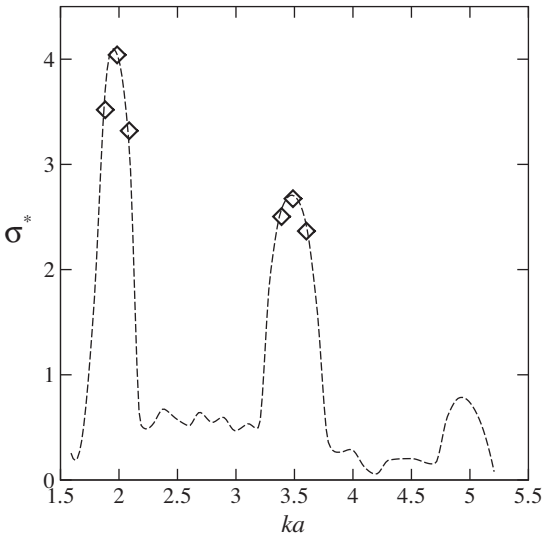

Fig. 2. Instability growth rates for $\Lambda = 1.0$ and $a/b = 0.14$ at $Re = 14000$. The dashed line is from the extracted results of [26] and ◇ is computed by the current code.

(defined as the mode with the largest growth rate) is calculated using an Implicitly Restarted Arnoldi Method as described by Sorensen [21].

Spatial discretisation of the domain was achieved using a spectral-element technique, which, through the use of high-order interpolation polynomials, allows highly accurate simulations (as described by Karniadakis et al. [22]). A third-order time accurate technique was employed to model the solution of the Navier–Stokes equations (see, [22]). This algorithm has previously been employed to model two-dimensional wake vortex dynamics by Sheard et al. [23]; while the linear stability analysis algorithm was successfully employed to resolve aspects of the three-dimensional transition of cylinder wakes in [24,25].

The spatial accuracy was determined at run time by choosing the order of the tensor-product of interpolating polynomials within each element. In all simulations quoted herein 441 elements, with polynomial of degree 10, were employed and a non-dimensional time-step, $\Delta t^* (= \Delta t a_0^2/\Gamma_2) = 1/9000\pi$ was used. A square domain was considered with a domain length and width of 100 vortex diameters. The vortex pair was contained within a refined region at the center of the mesh. Away from this region, the mesh density was reduced to reduce computational expense. This numerical configuration was used and found to be stable for all simulations in this investigation.

The algorithm employed was further tested by comparison with the findings from a similar investigation by Roy et al. [26]. The short-wave instability for a co-rotating equal-strength vortex pair ($\Lambda = 1.0$) was considered on a non-inertial reference frame in the test case. The simulation was conducted with a spatial resolution of both degree 10 and 13 polynomials on the current mesh. Extracted results from the prior study (Fig. 1 in [26]) are directly compared to the linear stability prediction of the current algorithm in Fig. 2. The non-dimensional growth rate is scaled as $2\pi^2 b^2 \sigma/\Gamma$ and a is estimated with Eq. (3). Differences of less than 0.1% are found when comparing both the degree 10 and 13 predictions with the results of [26]. This validation demonstrates that the present formulation correctly handles the rotating reference frame of the perturbation field, and confirms that accurate results are obtained when elements of polynomial degree 10 are used. This resolution is used for the remainder of this study.

2. Results

A flow field consisting of two circular vortices placed a finite distance apart is not a solution to the Navier–Stokes equations, and would not be observed experimentally. In order to generate an experimentally valid flow field, the initial flow field is evolved in two dimensions such that the solution relaxes to a solution of the Navier–Stokes equations. This relaxation process is driven by the strain rate within the core of each vortex evolving due to the external strain field generated by the other vortex, and is an inviscid process. The process has been described in detail for an unequal strength vortex pair in [18].

Fig. 3 shows contours of vorticity for the adapted vortex pair for several values of Λ. As $\Lambda \to 0$, the weaker vortex becomes increasingly deformed, and the profile of each vortex is increasingly different to that of the other vortex. [18] has shown that the time required for the adaptation process to conclude is dependent on Λ. Table 1 details the average core size of each vortex for selected values of Λ at the conclusion of the relaxation process. We note that as $|\Lambda| \to 0$, a discrepancy develops in the relative core sizes. The weaker vortex is stretched under the induced strain of its counterpart (see especially Fig. 3(a) and (b). This increases the characteristic average core size (computed according to [18,19]).

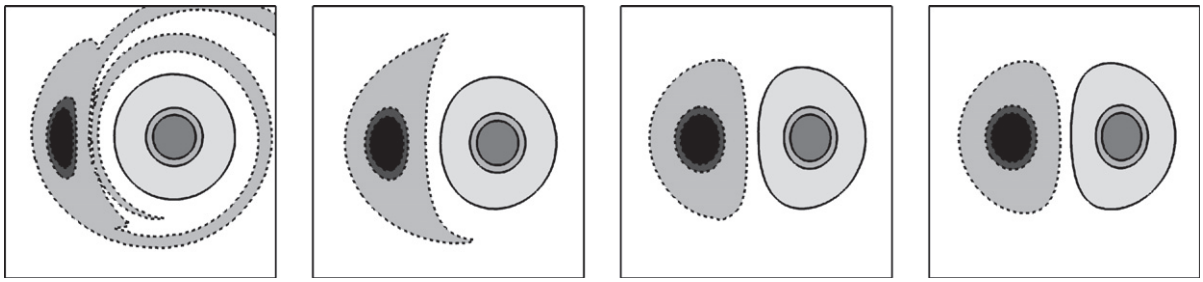

(a) $\Lambda = -0.1$ (b) $\Lambda = -0.3$ (c) $\Lambda = -0.7$ (d) $\Lambda = -0.9$

Fig. 3. Vorticity contour snapshots show vorticity profiles after relaxation. Solid and dashed lines represent positive and negative vorticity, respectively.

Table 1
Vortex core size at the conclusion of the adaptation phase, as a function of Λ.

Λ	a_1/b	a_1/a_0	a_2/a_0
−0.3	0.2677	1.0958	1.2860
−0.7	0.2731	1.1144	1.1544
−0.9	0.2748	1.1224	1.1317
−1.0	0.2761	1.1258	1.1258

2.1. Three-dimensional instability growth rates

Fig. 4 shows the normalized growth rate, σ^* of the leading instability mode as a function of the normalized wavenumber, ka_0, for $\Lambda = -0.9$. Four dominant instability modes have been identified. At low wavenumbers, the Crow instability is observed at $ka_0 \approx 0.1$, in close agreement with the analytical findings of [12]. The normalized growth rate is slightly lower than their findings due to the effect of viscosity (not accounted for in their model). The next mode is an oscillatory mode with a peak at $ka_0 \approx 1.1$. This mode has been identified in [27] for a $\Lambda = -1.0$ vortex pair and is characterized by a temporally oscillating perturbation field, that is contributed by the first solution branch of Kelvin mode $(-2,0)$.

Two further instability modes are also observed at higher wavenumbers, the first, with a peak at $ka_0 = 2.1$, is identified as the first solution branch of Kelvin mode $(-1,1)$. The second, with a peak at $ka_0 = 3.55$, is identified as the second solution branch of Kelvin mode $(-1,1)$. When comparing these results with [14], we find that both the peak growth rate for each mode, and the wavenumber at which this occurs, are very similar to the case of $\Lambda = -1.0$. The numerical result of the most unstable Kelvin mode is also directly compared with the theoretical prediction, based on the model of [14], for the weaker

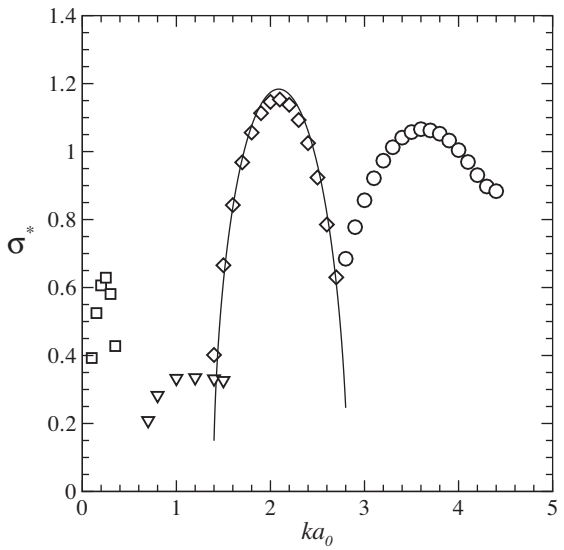

Fig. 4. Normalized instability growth rate as a function of ka_0 for $\Lambda = -0.9$. Symbols indicate different mode-shapes; ○ Crow instability; ▽ Kelvin mode $(-2,0,1)$; ◇ Kelvin mode $(-1,1,1)$; □ Kelvin mode $(-1,1,2)$. Solid line is predicted by the analytical model of [14] for the weak vortex.

vortex. Excellent agreement is achieved for the instability bandwidth and the peak growth rate. Both Kelvin $(-1,1)$ modes have substantially higher growth rates than the Crow instability or the Kelvin $(-2,0,1)$ mode, and should dominate the flow experimentally. However, both the instability types (Crow instability and the Kelvin modes $(-1,1)$) may be observed concurrently under experimental conditions [2] due to the large discrepancy in the their critical wavelengths.

Fig. 5 shows the instability growth rates for $\Lambda = -0.7$. All four modes identified for $\Lambda = -0.9$ are observed once again. The growth rate and the critical axial wavenumber of the most unstable Kelvin mode remains in good agreement with the theoretical prediction. The Crow instability is found to have a higher growth rate (compared to $\Lambda = -0.9$), with a peak growth rate occurring at a higher wavenumber, in agreement with the findings of [12]. In this case, the Kelvin mode $(-2,0,1)$ also has a higher growth rate (and a higher critical wavenumber). However, its peak growth rate is far less than all other instability modes observed. The Kelvin mode instabilities of $(-1,1)$ are also observed to have peak growth rates occurring at higher wavenumbers when compared with $\Lambda = -0.9$. However, their peak growth rates are reduced when compared with $\Lambda = -0.9$. This trend is continued as the circulation strength ratio magnitude is further reduced to $\Lambda = -0.3$ (Fig. 6). In this case, only the Crow instability and the first branch of the Kelvin mode $(-1,1,1)$ are observed as the principal leading modes across the range of wavenumbers considered. The oscillatory mode is also identified but is now a secondary mode. Here, the

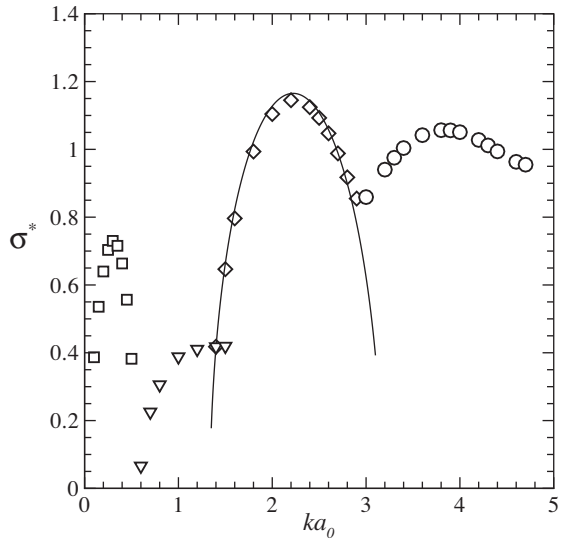

Fig. 5. Normalized instability growth rate as a function of ka_0 for $\Lambda = -0.7$. Symbols and the line are as per Fig. 3.

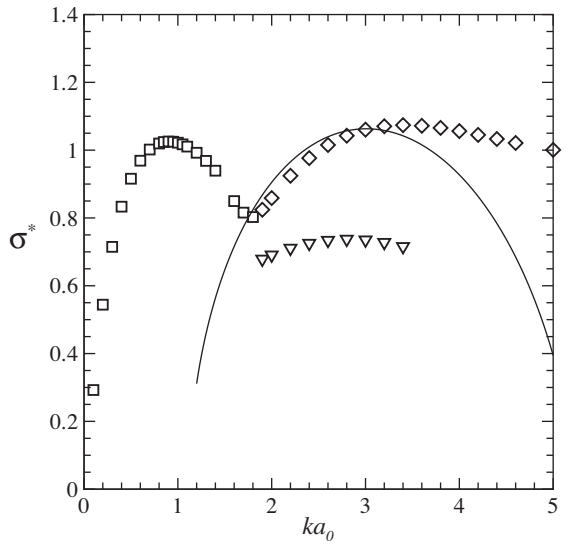

Fig. 6. Normalized instability growth rate as a function of ka_0 for $\Lambda = -0.3$. Symbols and the line are as per Fig. 3.

Crow instability peak growth rate has increased to the point where it is comparable to that of the Kelvin mode $(-1,1,1)$. The range of wavenumbers over which the Kelvin mode $(-1,1,1)$ has a significant growth rate is observed to be much broader than that observed at higher magnitudes of Λ. The theoretical model of [14] fails to provide reasonable predictions at higher wavenumbers. It is presumed that this is most likely due to the finite small strain assumption in the model and the extremely deformed weak vortex observed as $\Lambda \to 0$ (Fig. 2(a) and (b)).

Two summary figures are provided as Fig. 7 showing the magnitude and the critical wavenumber of the peak growth rates, both as a functon of Λ. The Kelvin instability mode $(-1,1,1)$ is observed to reduce in growth rate as $\Lambda \to 0$ (Fig. 7(a)), and is observed to have an increase in the normalized critical wavenumber (Fig. 7(b)). This is counter-intuitive, as the core radii of the weak vortex is greater as $|\Lambda| \to 0$. Therefore it is concluded that the increase in normalized mode wavenumber as $|\Lambda| \to 0$ is due to the increasing strain acting on the weak vortex profile as observed in Fig. 2. By contrast, the long wave-length, Crow instability displays an increase in growth rate as Λ decreases. This mode becomes more dominant than the Kelvin mode $(-1,1,1)$ at $\Lambda \approx -0.25$ and reaches a peak growth at $\Lambda \approx -0.15$, before decreasing in growth rate. In line with the short wave-length Kelvin modes, the Crow instability also exhibits an increase in normalized wavenumber with decreasing Λ. When $\Lambda < -0.2$, the Crow instability remains the only leading instability found. The Kelvin mode $(-2,0,1)$ exhibits an increase in the peak growth rate as $|\Lambda| \to 0$, in additional to an increase in the critical wavenumber. The growth rate of the Kelvin mode $(-2,0,1)$ reaches its maximum at $\Lambda \approx -0.15$ and decreases afterward, in line with the Crow instability. Logically, the growth rate of both the Crow instability and the Kelvin mode $(-2,0,1)$ is expected to drop towards zero as $|\Lambda| \to 0$, representing the case of a single, isolated vortex.

The mode shapes for each instability, calculated at the normalized wavenumber corresponding to maximum growth, are shown in Figs. 8–10. The images are taken in a two-dimensional horizontal cross-section which is at an arbitrary axial position. In each case, the perturbation field for both vortex cores are shown.

Fig. 8(a)–(e) shows the instability mode-shapes for $\Lambda = -0.9$. As both vortices have very similar circulation strengths, we may expect that the instability mode shapes may be near identical on each vortex – this is despite the fact that the perturbation mode-shape forms from a random perturbation field. Indeed, for the Crow instability (as shown in Fig. 8(c)), the mode shape growing on each vortex does appear of equal strength. This mode shape induces a sinuous oscillation along the axis of both vortices. The mode structure of the Crow instability is observed to occur on a scale larger than the vortex core, with a peak in ω_z observed on the vortex core radius. By contrast, all the Kelvin modes have smaller scale structures and are highly dependent on the profile of the base vortex. The oscillatory Kelvin mode $(-2,0,1)$ is shown in Fig. 8(d) and (e). The perturbation field of this mode is found to oscillate temporally between the state of (d) and (e). This mode can present as either a standing wave or a travelling wave (travelling in the axial direction) [28,29]. Comparing the mode shapes observed by Lacaze et al. [16], Billant et al. [27], we assume that the mode presents as a travelling wave. The perturbation vorticity (the mode shape) of the Crow instability is observed to be slightly reduced on the strong vortex. By contrast, all the Kelvin modes show an obvious reduction of perturbation vorticity strength in the strong vortex when compared with the weak vortex. This is especially apparent in the Kelvin mode $(-2,0,1)$ and the second solution branch of the Kelvin mode $(-1,1)$. It is postulated that the increased damping of the Kelvin modes (relative to the Crow instability) is due to the highly complex,

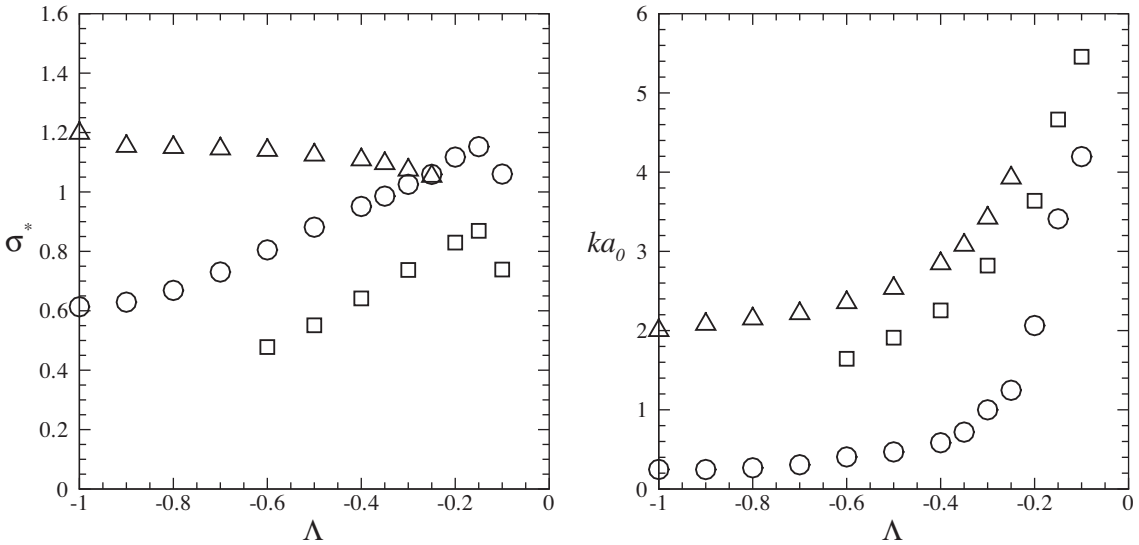

(a) Maximum σ^* (b) ka_0 of maximum growth

Fig. 7. Peak growth rates (linear regime) and the corresponding critical wavenumbers of the predicted instabilities at $Re = 20000$. △ Mode $(-1,1,1)$; ○ Crow instability; □ Mode $(-2,0,1)$.

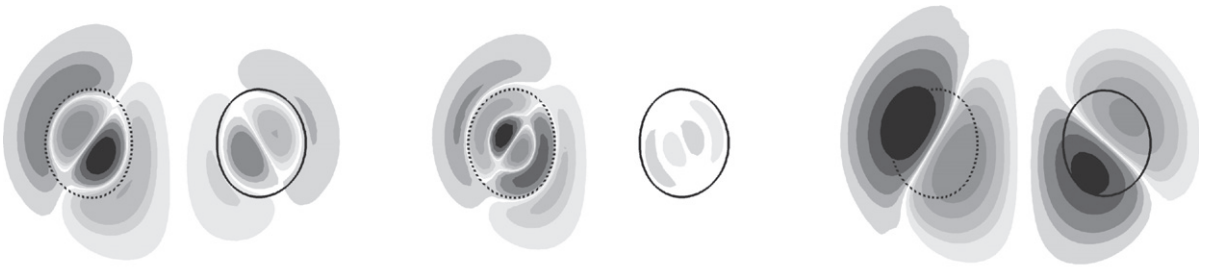

(a) Mode $(-1, 1, 1)$ at $ka_0 = 2.0$ (b) Mode $(-1, 1, 2)$ at $ka_0 = 3.6$ (c) Crow instability at $ka_0 = 0.25$

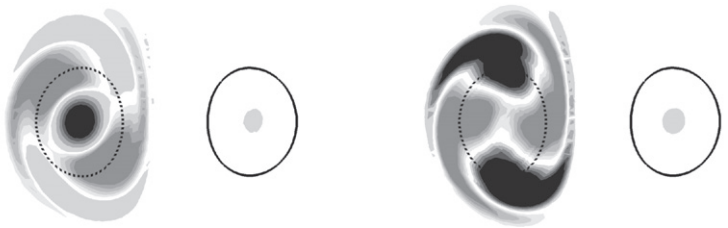

(d) Mode $(-2, 0, 1)$ at $ka_0 = 1.00$ (e) Mode $(-2, 0, 1)$ at $ka_0 = 1.00$

Fig. 8. Perturbation vorticity fields illustrating the mode shapes, corresponding to peak growth rates, identified for $\Lambda = -0.9$. Contour lines represent vorticity level of 0.33% of the local peak vorticity at each vortex. Darker flooded contours represent positive vorticity perturbations and lighter flooded contours represent negative vorticity perturbations.

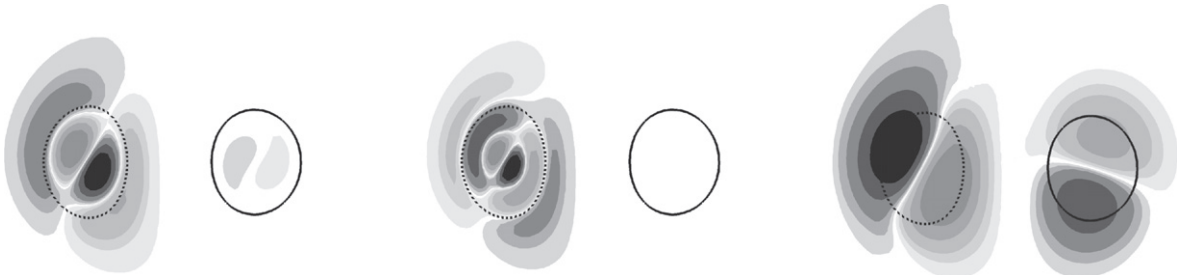

(a) Mode $(-1, 1, 1)$ at $ka_0 = 2.2$ (b) Mode $(-1, 1, 2)$ at $ka_0 = 3.8$ (c) Crow instability at $ka_0 = 0.3$

Fig. 9. Perturbation vorticity fields illustrating the mode shapes, corresponding to peak growth rates, identified for $\Lambda = -0.7$. Contour lines and flooded contours are as per Fig. 8.

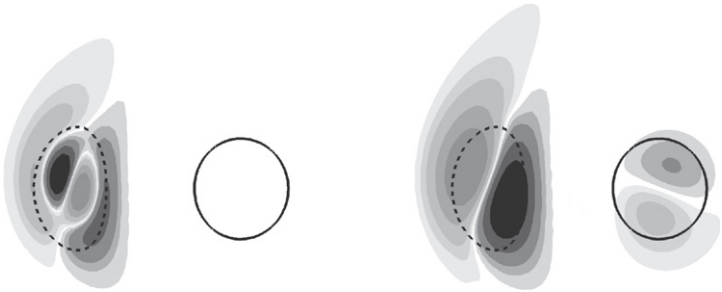

(a) Mode $(-1, 1, 1)$ at $ka_0 = 3.4$ (b) Crow instability at $ka_0 = 0.8$

Fig. 10. Perturbation vorticity fields illustrating the mode shapes, corresponding to peak growth rates, identified for $\Lambda = -0.3$. Contour lines and flooded contours are as per Fig. 8.

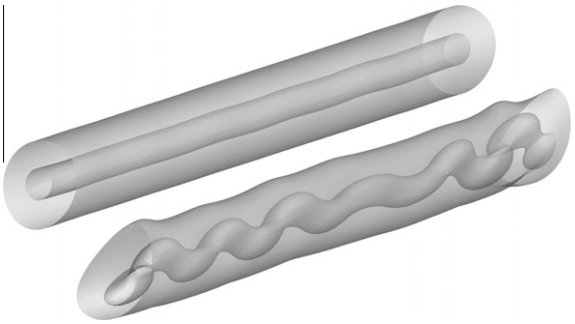

Fig. 11. Direct numerical simulation of a $\Lambda = -0.6$ vortex pair at $Re = 2400$. Two levels of vorticity iso-surface are plotted for each vortex. The weaker vortex is the lower vortex in this figure.

small-wavelength structures inherent with these modes. By comparison, the large wave-length, Crow instability has a relatively simple structure, with larger scales in all three dimensions.

The strain at the center of the strong vortex decreases with $|\Lambda|$ [18]. Thus, for the case $\Lambda = -0.7$, the perturbations do not develop as vigorously on the strong vortex, when compared with the case of $\Lambda = -0.9$. Indeed, at $\Lambda = -0.7$, only the Crow mode develops any appreciable perturbations on the strong vortex as shown in Fig. 9(c). Comparing $\Lambda = -0.7$ with $\Lambda = -0.9$, it is interesting to note that the mode-shapes in the weak vortex in Fig. 9 have not altered appreciably with Λ. As $|\Lambda|$ is further reduced to $\Lambda = -0.3$, only two instability modes are observed as the leading modes across the wavenumber domain. Their perturbation fields are shown in Fig. 10(a) and (b). A finite amount of perturbation vorticity still appears in the vicinity of the strong vortex for the Crow instability, but no perturbation is observed to grow on the stronger vortex for the Kelvin mode $(-1,1,1)$.

Considering Fig. 7(b), we note that the peak growth of the Kelvin mode $(-1,1,1)$ occurs at higher normalized wavenumber as $|\Lambda| \to 0$. The bandwidth of this mode has also been shown to become broader in Figs. 4–6. Given the higher growth rate of the first solution branch of the Kelvin mode, it is not surprising that the second branch solution is not observed for $\Lambda = -0.3$. The mode structure for the first solution branch of the Kelvin mode only appears on the highly strained, weak vortex. The strain of the base field has appreciably altered the mode shape in Fig. 10(a). This is also apparent for the Crow instability that also grows more strongly on the weak vortex in preference to the strong vortex in Fig. 10(a).

A plot from a three-dimensional direct numerical simulation for a $\Lambda = -0.6$ vortex pair is shown in Fig. 11. The overall domain has a length of roughly six critical instability wavelengths. At the time shown in the plot, non-linear growth of the mode is just becoming evident. The core of the weaker vortex is seen to be more heavily deformed than the stronger vortex due to the three-dimensional instability. The typical sinusoidal core structure [2,5] is observed inside the weaker vortex and is believed to be driven by the Kelvin mode $(-1,1)$. This result supports our prediction that perturbations are stronger on the weaker vortex.

3. Discussion

Large wavelength Crow instabilities begin to dominate as $|\Lambda| \leqslant 0.25$. We note an increase in growth rate and critical wavenumber for this mode for smaller $|\Lambda|$, in agreement with analytical findings of [12]. Analytical evaluations of the Crow instability do not consider the effects of highly deformed core profile on the development of the mode. Despite this, the severe deformation of the weak vortex noted for small $|\Lambda|$ has little influence on the mode development, in agreement with their findings.

By contrast, the growth of the short-wavelength Kelvin modes is highly dependent on the vortex profile. Slight deviations away from $|\Lambda| = 1$ results in a significant asymmetry in instability mode development across the vortex cores. We note that even for $\Lambda = -0.9$, a significant difference is observed in the amplitude of the perturbation mode-shape growing on the weak vortex by comparison to the strong vortex. This is especially apparent for the second branch of the Kelvin mode $(-1,1)$ of more complicated structure, as well as the Kelvin mode $(-2,0,1)$. In closing it should be stated that the linear instabilities observed, in isolation, do not cause any appreciable reduction in the coherence of either vortex core. However, they are the leading instability modes in a cascade that is expected to significantly decrease the coherence of the vorticity making up the vortex pair. The linear perturbation mode-shape is critical to further non-linear instability developments. Enhanced dissipation of a vortex pair requires the development of instability modes on both vortex cores. In the absence of this, one vortex will remain coherent while the other is destroyed. For practical applications (in particular for aircraft wakes), these findings indicate that each vortex making up a vortex pair should have similar circulation strength to ensure that the dissipation of both vortices is enhanced. In addition, it is of interest that the normalized growth rate decreases for all modes for $|\Lambda| < 0.2$, indicating that there is a critical value of $|\Lambda|$, below which instabilities on the weaker vortex develop more slowly. Further investigations of direct numerical simulation are required to elucidate the non-linear instability growth that occurs beyond the linear growth regime.

4. Conclusion

A linear stability analysis of counter-rotating vortex pairs with unequal circulation strengths has been conducted. Three instability modes have been identified across the range $-0.1 > \Lambda > -1.0$. These modes are equivalent to instability modes described in previous studies of equal strength counter-rotating vortex pairs, and features a Crow instability and two Kelvin modes. However, in this case, Kelvin mode instabilities are observed to grow preferentially on the weaker vortex, and the global growth rate of these Kelvin modes $(-1,1)$ reduces as $|\Lambda| \to 0$. By contrast the long wave-length Crow instability and another Kelvin mode $(-2,0,1)$ exhibit an increase in growth rate as $|\Lambda|$ is reduced. In addition, the Crow instability exhibits strong growth on both vortex cores down to $\Lambda = -0.3$. These linear instability modes may lead to enhanced dissipation of the vortex pair.

References

[1] L. Jacquin, D. Fabre, D. Sipp, V. Theofilis, H. Vollmers, Instability and unsteadiness of aircraft wake vortices, Aerosp. Sci. Technol. 7 (2003) 577–593.
[2] T. Leweke, C.H.K. Williamson, Cooperative elliptic instability of a vortex pair, J. Fluid Mech. 360 (1998) 85–119.
[3] S.C. Crow, Stability theory for a pair of trailing vortices, AIAA J. 8 (1970) 2172–2179.
[4] C.Y. Tsai, S.E. Widnall, Stability of short waves on a straight vortex filament in a weak externally imposed strain field, J. Fluid Mech. 73 (1976) 721–733.
[5] F. Laporte, A. Corjon, Direct numerical simulations of the elliptic instability of a vortex pair, Phys. Fluids 12 (2000) 1016–1031.
[6] R.T. Pierrehumbert, Universal short-wave instability of two-dimensional eddies in an inviscid fluid, Phys. Rev. Lett. 57 (1986) 2157–2159.
[7] B.J. Bayly, 3-dimensional instability of elliptical vortex, Phys. Rev. Lett. 57 (1986) 2160–2163.
[8] S.E. Widnall, J.P. Sullivan, Stability of vortex rings, Proc. R. Soc. London. Ser. A, Math. Phys. Sci. 332 (1973) 335–353.
[9] S.E. Widnall, D.B. Bliss, C.Y. Tsai, Instability of short waves on a vortex ring, J. Fluid Mech. 66 (1974) 35–47.
[10] R.R. Kerswell, Elliptic Instability, Annu. Rev. Fluid Mech. 34 (2002) 83–113.
[11] J.M. Ortega, R.L. Bristol, Ö. Savas, Experimental study of the instability of unequal-strength counter-rotating vortex pairs, J. Fluid Mech. 474 (2003) 35–84.
[12] R.L. Bristol, J.M. Ortega, P.S. Marcus, o. Şavas, On cooperative instabilities of parallel vortex pairs, J. Fluid Mech. 517 (2004) 331–358.
[13] J.D. Crouch, Instability and transient growth for two trailing-vortex pairs, J. Fluid Mech. 350 (1997) 311–330.
[14] S. Le Dizès, F. Laporte, Theoretical predictions for the elliptical instability in a two-vortex flow, J. Fluid Mech. 471 (2002) 169–201.
[15] D. Sipp, L. Jacquin, Widnall instabilities in vortex pairs, Phys. Fluids 15 (2003) 1861–1874.
[16] L. Lacaze, K. Ryan, S. Le Dizès, Elliptic instability in a strained Batchelor vortex, J. Fluid Mech. 577 (2007) 341–361.
[17] L. Kelvin, Vibratons of a columnar vortex, Phil. Mag. 344 (1880) 181–212.
[18] J. So, K. Ryan, G.J. Sheard, Interaction of an unequal-strength vortex pair, in: Proceedings of the 16th Australasian Fluid Mechanics Conference (Pub: School of Engineering, The University of Queensland, ISBN: 978-1-864998-94-8), 2, 2007, p. 7.
[19] S. Le Dizès, A. Verga, Viscous interactions of two co-rotating vortices before merging, J. Fluid Mech. 467 (2002) 389–410.
[20] L.K. Brandt, T.K. Cichocki, K.K. Nomura, Asymmetric vortex merger: mechanism and criterion, Theor. Comput. Fluid Dyn. (2009) 1–5.
[21] D.C. Sorensen, Implicitly restarted Arnoldi/Lanczos methods for large scale eigenvalue calculations, in: D.E. Keys, A. Sameh, V.V. (Eds.), Parallel numerical algorithms, Kluwer, Dordrecht, 1995.
[22] G.E. Karniadakis, M. Israeli, S.O. Orszag, High-order splitting methods for the incompressible Navier Stokes equations, J. Comput. Phys. 97 (1991) 414–443.
[23] G.J. Sheard, T. Leweke, M.C. Thompson, K. Hourigan, Flow around an impulsively arrested circular cylinder, Phys. Fluids 19 (2007) 083601.
[24] G.J. Sheard, M.J. Fitzgerald, K. Ryan, Cylinders with square cross-section: wake instabilities with incidence angle variation, J. Fluid Mech. 630 (2009) 43–69.
[25] H.M. Blackburn, G.J. Sheard, On quasiperiodic and subharmonic Floquet wake instabilities, Phys. Fluids 22 (2010) 031701.
[26] C. Roy, N. Schaeffer, S. Le Dizès, M. Thompson, Stability of a pair of co-rotating vortices with axial flow, Phys. Fluids 20 (2008) 094101.
[27] P. Billant, P. Brancher, J. Chomaz, Three-dimensional stability of a vortex pair, Phys. Fluids 11 (1999) 2069–2077.
[28] H.M. Blackburn, J.M. Lopez, On three-dimensional quasiperiodic Floquet instabilities of two-dimensional bluff body wakes, Phys. Fluids 15 (2003) L57.
[29] H.M. Blackburn, J.M. Lopez, The onset of three-dimensional standing and modulated travelling waves in a periodically driven cavity flow, J. Fluid Mech. 497 (2003) 289–317.